Bragg reflection spectroscopy of opal-like photonic crystals

G. M. Gajiev,* V. G. Golubev, D. A. Kurdyukov, A. V. Medvedev, A. B. Pevtsov, A. V. Sel'kin, and V. V. Travnikov†
Ioffe Institute, Russian Academy of Sciences, 194021 St. Petersburg, Russia
(Received 19 May 2005; published 15 November 2005)

We have studied Bragg reflection spectra of photonic crystals based on synthetic opals. The samples under study represented opal-semiconductor composites, in which the opal pores were filled with GaN and GaP, and GaN-inverted structures with the opal matrix removed from the composite. Bragg reflection spectroscopy is found to possess new capabilities for characterization of opal-like structures. A theoretical approach to the reflectance spectrum analysis has been developed on the assumption of a planar spatially periodic medium, accounting for the effects of sintering of SiO_2 opal spheres and their uniaxial strain. For an additional characterization of the samples, we considered a structural invariant relating to each other the photonic crystal lattice parameters and the spectral positions of features in multiple Bragg diffraction spectra.

DOI: 10.1103/PhysRevB.72.205115 PACS number(s): 42.25.Fx, 42.70.Qs, 78.20.Bh, 81.05.Zx

I. INTRODUCTION

A photonic crystal (PhC) is a bulk spatially periodic structure whose dielectric constant is modulated with a period comparable to the light wavelength. The interaction between such a crystal and photons essentially modifies the spatial distribution and the energy spectrum of the electromagnetic field. In particular, photonic band gaps can arise, in which light cannot propagate along certain directions (pseudogap, or stop band) or along all the directions (full gap).[1] Current interest in PhCs is due to the possibility of studying some fundamental aspects of quantum electrodynamics and because these structures are promising for various applications in laser and telecommunication technologies.[2,3] Of special value are PhCs with a three-dimensional (3D) translation symmetry since they can possess a full gap.[4–6]

A common material used for fabrication of 3D PhCs is synthetic opal. Its face-centered-cubic (fcc) lattice is made up of close-packed submicron spheres of amorphous silica, a-SiO_2. A sublattice of interconnected pores occupies the space between the spheres. The pores can be filled with various substances to create a great variety of 3D PhC modifications. The filling with semiconductor compounds produces crystalline photonic composites of the opal-semiconductor type.[7–9] These combine the unique properties of a 3D periodic opal structure and the specific optical and electrical properties of a semiconductor. By using semiconductors with various forbidden gap widths and by varying the semiconductor filling fraction, one can deliberately change the fundamental properties of photonic crystals.

A direct control of pore filling during the composite fabrication is a hard task. On the other hand, the way the pores are filled may considerably affect the PhC properties, so one should keep this in mind when making quantitative evaluations. Note that the incorporation of a semiconductor material into opal pores normally occurs at high temperatures. The sample heating may lead to additional sintering (an increase in the contact area) of the a-SiO_2 spheres and to a change in their geometry, making them, for example, ellipsoidal. Anisotropic sintering and deformation of the spheres may modify the point symmetry and, hence, the optical characteristics of the PhC.[10–13] Moreover, we can expect a frequency variation of the dielectric constant to arise in the filler material, especially in the spectral region of the fundamental absorption edge. Therefore, there is the necessity to gain a better insight into the mechanisms of PhC optical spectra, taking into account their structural modifications and dielectric properties. It is also important to improve available methods of optical spectroscopy for PhC characterization.

The present paper demonstrates the diagnostic capabilities provided by the analysis of Bragg reflection (BR) spectra of 3D opal-based PhCs filled with various materials. The experimental data are analyzed in terms of specific optical properties of the fillers and possible deformation of the crystal structure. We have studied unfilled synthetic opals, opals filled with immersion liquids (water, glycerol), opals with the wide-gap semiconductors GaN and GaP synthesized in the pores, as well as inverted structures, in which the spheres are air, and interstitial regions are filled with a semiconductor. These PhCs are fabricated by removing opal template from the opal-semiconductor composite.

II. EXPERIMENTAL

A. Samples

The initial host crystals used for fabricating PhCs were synthetic opals (see also Refs. 14–18) composed of 3D ordered lattices of close-packed a-SiO_2 spheres of submicron size with the diameter variation of ~5%. The volume of the air pores among the spheres may be as large as 26% of the total volume available for filling with other substances. The sphere diameters were preliminarily found with a scanning electron microscope (SEM) to be about 260–270 nm.

The samples to be studied were made as plates of 5×5 mm^2 in size and ~0.5 mm thick. They were cut out in such a way that the largest sample surface would coincide with the (111) reflecting plane. The opal pores were filled with the immersion liquids or semiconductors (GaN and GaP) synthesized directly in the pores, following a technology similar to that described in Refs. 15–18. The temperature was 950 °C for the GaN synthesis and 800 °C for GaP. The filling procedure left the sample surface totally continuous and consisting only of the semiconductor material to be pol-

ished off prior to the spectroscopic measurements. To obtain inverted structures, i.e., PhCs consisting totally of the semiconductor material, the opal matrix was etched off the composite by using an aqueous solution of fluoric acid.

B. Bragg reflection spectra

The analysis of BR spectra is a simple and direct method for studying the PhC band structure. The reflection peaks arise from Bragg diffraction of light on the families of PhC crystal planes and correspond to the photon energies and wave vectors, for which light propagation through an ideal PhC is forbidden. An important characteristic of a PhC is the stop-band width ΔE_{gap} governed by the spatial modulation percentage of the dielectric constant varying with the dielectric contrast q of the materials comprising the PhC. When a PhC is made up of two spatially alternating materials a and b, the parameter q can be defined as

$$q = (\varepsilon_a - \varepsilon_b)/(\varepsilon_a + \varepsilon_b),$$

where ε_a and ε_b are the respective dielectric constants of the materials. For an opal-like PhC, ε_a will be taken to mean the dielectric constant of the spheres ("atoms") and ε_b the dielectric constant of the pores. In the initial host crystal, we have $\varepsilon_b = 1$, i.e., the pores are filled with air and $\varepsilon_a > \varepsilon_b$, such that $0 < q < 1$. Opal-semiconductor composites and inverted structures normally obey the opposite inequality, $\varepsilon_a < \varepsilon_b$; thus, we have $-1 < q < 0$.

The value of ΔE_{gap} for highly contrast structures is sometimes found experimentally as full width at half maximum (FWHM) ΔE_{FWHM} of the spectral band.[19] In order to compare the photonic properties of various composites, it is convenient to use the relative width $\Delta E_{\text{FWHM}}/E_0$ of the reflex (E_0 is the energy at the reflection peak), measured at normal light incidence on the family of crystal planes.

The synthetic opal samples chosen for semiconductor filling demonstrated well-defined BR peaks. Their analysis allowed us to preliminarily characterize the structure of the initial 3D host crystals. Such a characterization appears quite reasonable since the semiconductor compound synthesized in opal pores cannot be said to have been fully described as to its optical properties or filling fraction. Of special interest among the PhC characteristics of initial opals are their spatial periods determined by the size and arrangement of the a-SiO_2 spheres, as well as their dielectric constants.

To obtain reliable information on the geometry and dielectric parameters of the initial opals, we measured the BR spectra of pure opals and those filled up with water or glycerol, the two liquids with well-known dielectric constants.[20]

The use of water or glycerol as fillers decreases considerably the contrast in the spatially periodic medium because of the close values of the dielectric constants of the opal spheres and the immersion liquids.[21,22] As a result, the BR peaks for the opal-water and opal-glycerol systems become much narrower than those for the initial unfilled opal. This allows a precise identification of the spectral positions of the photonic band gaps and a successful application of Bragg's law of electromagnetic wave diffraction to the analysis of experimental data.

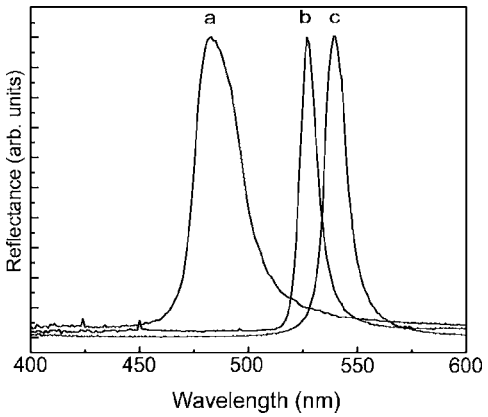

FIG. 1. Bragg light reflection spectra of (a) pure opal, (b) opals filled with water, and (c) glycerol.

Figure 1 illustrates the BR spectra for bare opal [Fig. 1(a)] and for samples filled with water and glycerol [Figs. 1(b) and 1(c), respectively]. The spectra were registered in s-polarized light at the incidence angle $\theta \approx 10°$, counted from the normal to the (111) sample plane. One can see that the filled samples do exhibit narrower reflexes than those of pure opal. The values of $\Delta E_{\text{FWHM}}/E_0$ for bare, water-filled, and glycerol-filled opals are found to be 0.047, 0.018, and 0.020, respectively. As the angle θ becomes larger, the reflection peaks are shifted toward the shorter wavelengths and the s component exhibits a broadened resonance reflection contour. The positions of the Bragg reflex peaks are shown in Fig. 2 as a function of the incidence angle (experimental points) for opal-glycerol (triangles) and opal-water (squares) samples. These angular dependences are well described by Bragg's formula

$$\lambda = 2d_{111}\sqrt{\varepsilon_0 - \sin^2\theta}, \tag{1}$$

where λ is the wavelength at the reflex peak, d_{111} is the spacing between adjacent [111] lattice planes, θ is the incidence angle, and ε_0 is the average dielectric constant of the composites:

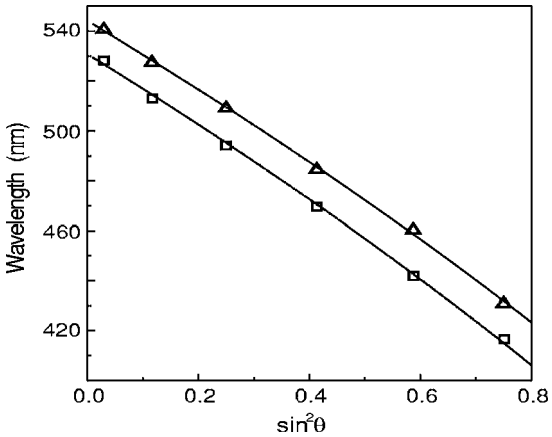

FIG. 2. The angular dependence of the peak positions of Bragg reflexes for opal-glycerol (triangles) and opal-water (squares) and calculations from Eq. (1) (solid curves).

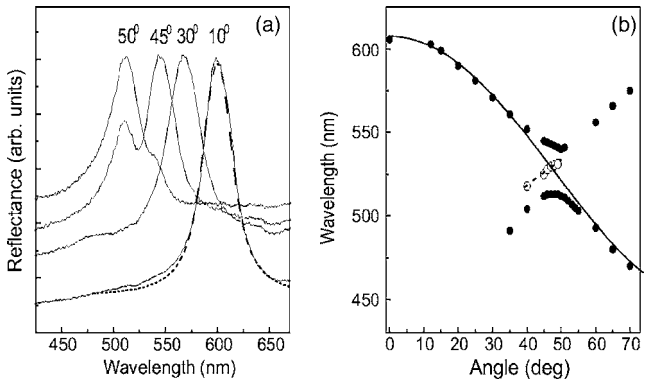

FIG. 3. Opal-GaN composites: (a) Bragg reflection spectra for various incidence angles of *s*-polarized light (solid curves) and the spectrum calculated at the angle of 10° (dashed curve); (b) the angular dependence of the peak positions of Bragg reflexes (full circles) and the dip positions in the doublets (open circles) with calculated peak positions for reflection by the (111) planes parallel to the sample surface (solid curve).

$$\varepsilon_0 = \varepsilon_a f_0 + \varepsilon_b (1 - f_0), \tag{2}$$

where f_0 is the filling fraction for the structure (the volume fraction of sphere material).

It should be noted that the filling fraction f_0 in the expression for the average dielectric constant can vary with the sample because of the different degrees of the sphere sintering in a particular structure. For the structure to acquire a sufficiently high hardness, f_0 must be larger than ~ 0.74 for the fcc packing of spheres having point contacts.

The parameters of Eqs. (1) and (2) were calculated by the least-squares method, using the experimental data on the two dependencies in Fig. 2. The varying parameters were ε_a, d_{111}, and f_0. The dielectric constants for glycerol ($\varepsilon_b = \varepsilon_{gl} = 2.160$)[20] and water [$\varepsilon_b = \varepsilon_{H_2O} = 1.769$][20] were assumed to be fixed. The resulting values were found to be $\varepsilon_a = 1.98$,[36] $d_{111} = 190.8$ nm, and $f_0 = 0.749$.

Unlike the filling with the liquids, the semiconductor fillers yield a larger value of $|q|$. As a result, the photonic band gap becomes much wider, increasing the relative width of the reflection bands at normal light incidence: $\Delta E_{FWHM}/E_0 = 0.051$ for opal-GaN and $\Delta E_{FWHM}/E_0 = 0.11$ for GaN-inverted opal. The BR spectra also become different.[17,18] The PhC spectra of opal-GaN and inverted structures consisting totally of GaN are presented in Figs. 3 and 4. The samples were oriented in such a way that the wave vectors of the incident and reflected light were in the plane going through the points Γ, U, L, and K in the Brillouin zone of the fcc lattice. As the incidence angle increases, additional features of shorter wavelengths arise in the vicinity of $\theta \approx 30°$ in the spectra registered in the *s* polarization, as is seen in Figs. 3 and 4. The peak intensity increases gradually, and the features acquire a well-defined doublet geometry at $\theta \approx 35° - 55°$. As the angle increases further, the intensity of the long-wavelength feature becomes lower, eventually leaving a single short-wavelength peak. The dependence of the spectral positions of the BR features on the light incidence, presented in Figs. 3(b) and 4(b), allow identification of two

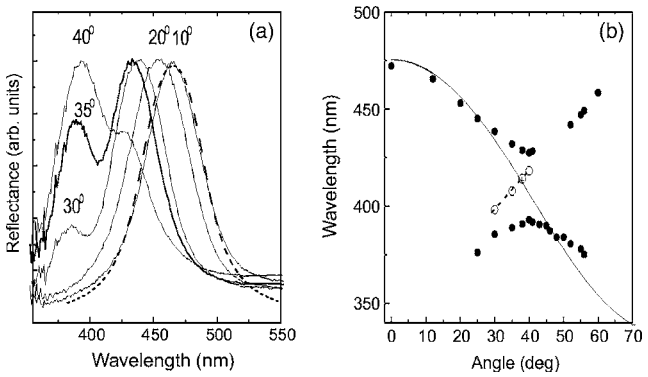

FIG. 4. GaN-inverted structures: (a) Bragg reflection spectra for various incidence angles of *s*-polarized light (solid curves) and the spectrum calculated at the incidence angle of 10° (dashed curve); (b) the angular dependence of the peak positions of Bragg reflexes (full circles) and the dip positions in the doublets (open circles), with the calculated peak positions of reflection by the (111) planes parallel to the sample surface (solid curve).

branches separated by an avoided crossing area.[23]

GaP crystals are known to have a large dielectric constant, at the absorption edge.[24] In totally inverted GaP PhCs, the optical contrast has been reported to be large enough for a full gap to arise.[25] The pores in the samples under study were only partially filled, but even there the value of q for an opal-GaP composite is quite large. This is clear from the largest relative width of the reflection band, $\Delta E_{FWHM}/E_0 = 0.16$, and from the behavior of the peak positions with increasing incidence (Fig. 5). The peak positions in the angle range up to $\sim 70°$ change but slightly, with the reflection bands partly overlapping each other at the minimum and maximum θ values.

The doublet structure in the reflection spectra at oblique incidence is due to multiple Bragg diffraction—a simultaneous light diffraction on, at least, two intercepting crystal planes.[23] Multiple diffraction radically changes the behavior of the peak positions as a function of the light incidence.

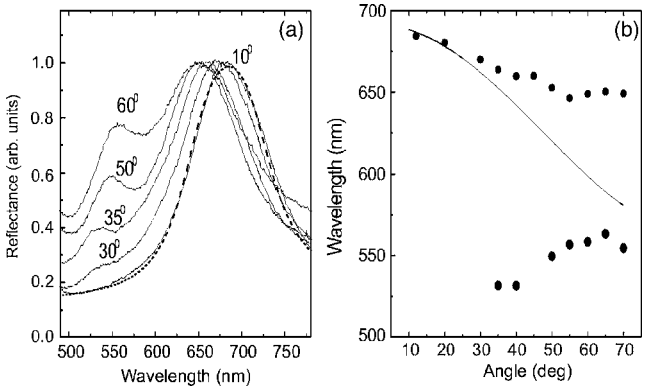

FIG. 5. Opal–GaP composites: (a) Bragg reflection spectra for various incidence angles of *s*-polarized light (solid curves) and the spectrum calculated at the angle of 10° (dashed curve); (b) the angular dependence of the peak positions of Bragg reflexes (full circles) with the calculated peak positions for reflection by the (111) planes parallel to the sample surface (solid curve).

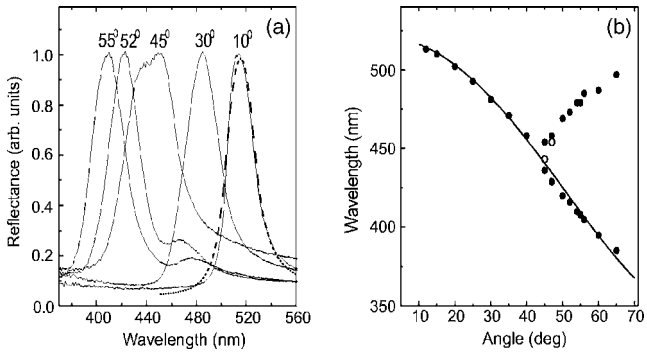

FIG. 6. Bare opal: (a) Bragg reflection spectra for various incidence angles of *s*-polarized light (solid curves) and the spectrum calculated at 10° (dashed curve); (b) the angular dependence of Bragg reflexes (full circles) and the dip positions in the doublets (open circles), with peak position of reflection by the (111) planes parallel to the sample surface (solid curve).

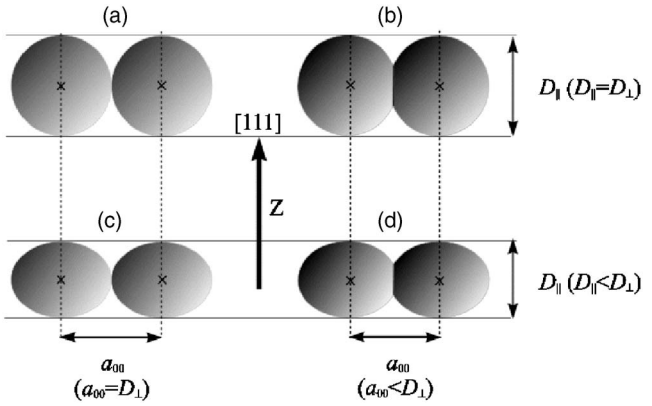

FIG. 7. The arrangement of neighboring point-contacted (a,c) and sintered (b,d) spheres (a,b) or spheroids (c,d) belonging to the (111) crystal plane of the opal structure.

This is clear from Figs. 3(b), 4(b), and 5(b) comparing the experimental peak positions and the positions calculated from formula (1) and indicated with a solid curve to be expected for common Bragg diffraction by the (111) planes parallel to the sample surface. The effect of multiple diffraction limits the characterization of opal-semiconductor composites, based on the simple procedure described above for liquid-filled opals.

In bare opals, the major peak positions are described well by Eq. (1) nearly in the whole range of incidence angles [Fig. 6(b)]. It is only in the narrow region of $\sim 44° - 46°$ that the spectra demonstrate a doublet behavior due to the multiple diffraction. Note that the doublet structure in both pure opal and opal-semiconductor composites is best pronounced in the above BR geometry, when the wave vectors of the incident and reflected beams lie in the plane with the points Γ, K, L, and U in the Brillouin zone.

III. THEORY

A. Strain in closed-packed cubic structures

One of the objectives of the present study was to develop procedures for finding optical and structural parameters of the samples from Bragg reflection spectra. To compare the calculated and experimental parameters, we considered a model crystal having a spatially periodic dielectric structure with dielectric spheres located at the lattice sites. This model accounts for the sintering effects of the structural elements—spheres—and their possible uniaxial strain along the [111] growth axis, which is responsible for turning them to ellipsoids. This kind of effect may occur in actual structures and has been observed in SEM micrographs (see, e.g., Refs. 10 and 12).

Possible pairs of the structural elements in an opal-like material are shown, schematically, in Fig. 7 for four types of structure: 7(a) with ideal spheres having a point contact 7(b) with interpenetrating (sintered) spheres, 7(c) with ideal point-contacted spheroids, and 7(d) with uniaxially compressed interpenetrating spheroids. Note that these combinations of the structural elements reflect their actual arrangement in a layer parallel to the outer (lateral) (111) plane of the photonic crystal and do not include the elements of the adjacent (111) layers, which are taken into account in the model.

Let us denote the axial lengths of close-packed ellipsoids as $D_{\|}$ and $D_{\perp}$, assuming them to be spheroidal and the $D_{\|}$ axis coinciding with the rotation axis normal to the reflecting plane. The distance a_{00} between the centers of neighboring spheroids having a point contact and located in the lateral plane is taken to be $D_{\perp}$. The spacing L between adjacent (111) lattice planes of the structure in the direction normal to the surface is described as $L=d_{111}=\sqrt{2/3}D_{\|}$. Because of sintering, the distance a_{00} decreases by Δa_{00} and L decreases by ΔL.

If we denote the relative change in the parameters a_{00} and L as the sintering coefficient $\chi=\Delta a_{00}/D_{\perp}=\Delta L/L$ (assuming the sintering to be isotropic), the filling fraction f_0 for moderately sintered spheroids ($\chi \leqslant 1-\sqrt{3}/2 \approx 0.134$) will take the form[26]

$$f_0 = f_{00}\frac{1-3\chi^2(3-\chi)}{(1-\chi)^3} \tag{3}$$

with $f_{00}=\pi/3\sqrt{2}\approx 0.74$. In the absence of sintering ($\chi=0$), we have $f_0=f_{00}$. This value is independent of the ratio of the axial lengths of the ellipsoid and describes, in particular, a cubic lattice of closed packed spheres at $D_{\|}=D_{\perp}$. The restriction imposed on χ ($\leqslant 0.134$) obeys the condition for the spatial separation of the interpenetration regions for various ellipsoidal pairs.

The ellipsoidal shape of the lattice constituents reduces the O_h symmetry of the structure to the D_{3d} symmetry, which is consistent with the uniaxial strain along the [111] direction, coinciding in our case with the normal to the surface. This strain can be quantitatively described by an anisotropic shrinkage coefficient

$$\eta = D_{\|}/D_{\perp} \tag{4}$$

B. Approximation of a planar spatially periodic medium

To analyze the BR spectra theoretically, we employed the approximation of a planar spatially periodic medium (a planar approximation).[27,28] Within this approach, a dielectric material possessing a 3D periodicity (in the case of interest, it is an opal-like PhC plate) is averaged along the directions parallel to the outer sphere layer, i.e., normal to the [111] direction coinciding with the Z axis of the coordinates. Since the averaging is made only along the X and Y axes, the dielectric constant becomes a periodic function $\varepsilon_s(z)$, depending only on the space variable z

$$\varepsilon_s(z) = \varepsilon_a f_s(z) + \varepsilon_b(1 - f_s(z)), \tag{5}$$

where $\varepsilon_s(z)$ is expressed through the effective filling function $f_s(z)$, which can be written for one period $0 \leqslant z \leqslant L$ in the form

$$f_s(z) = u(z) + u(z - L) \tag{6}$$

with

$$u(z) = \frac{\alpha_0^2}{\sqrt{3}(1-\chi)^2}\{2\pi + 6[\sin(2\beta_0) - 2\beta_0] + 3[\sin(2\beta_1) - 2\beta_1]\},$$

$$\alpha_0 = Re\ \sqrt{1/4 - (z/D_\parallel)^2},$$

$$\beta_i = \arcsin[Re\ \sqrt{1 - (\rho_i/\alpha_0)^2}], \quad (i = 0,1),$$

$$\rho_0 = \tfrac{1}{2}(1-\chi), \quad \rho_1 = \sqrt{3}\rho_0 - \sqrt{2}|z|/D_\parallel;$$

$$D_\parallel = \eta D_\perp, \quad D_\perp = \frac{a_{00}}{1-\chi},$$

$$L = D_\parallel\sqrt{2/3}(1-\chi) = a_{00}\eta\sqrt{2/3}.$$

In the expression for $u(z)$, the term containing β_0 defines the reduction in the f_s modulation percentage of due to the overlapping of an ellipsoid by six neighbors located in the same growth layer, whereas the term with β_1, also reducing the modulation percentage, describes the overlapping of this ellipsoid by three neighbors in the adjacent growth layer parallel to the lateral plane.

The effect of the boundary conditions was accounted for by truncating the spheroids in the outer layer of the PhC plate, such that the front surface v and the back surface u of the plate were considered as being shifted inward at a distance Δl_v and Δl_u, respectively, away from the outer planes contacting the untruncated spheroids. To describe the boundary conditions quantitatively, we introduced the cutoff factors $\zeta_v = 2\Delta l_v/D_\parallel$ and $\zeta_u = 2\Delta l_u/D_\parallel$ for the front and back surfaces, respectively.

The typical profiles $f_s(z)$ of the effective filling function calculated at different sintering coefficients [$\chi=0(1)$, $\chi=0.05(2)$ and $\chi=0.1(3)$] are shown in Fig. 8, with the number of periods along the [111] direction plotted along the abscissa: $N_p = z/d_{111}$. One can see that the modulation percentage of the function f_s decreases with increasing χ and that its profile changes essentially over a period.

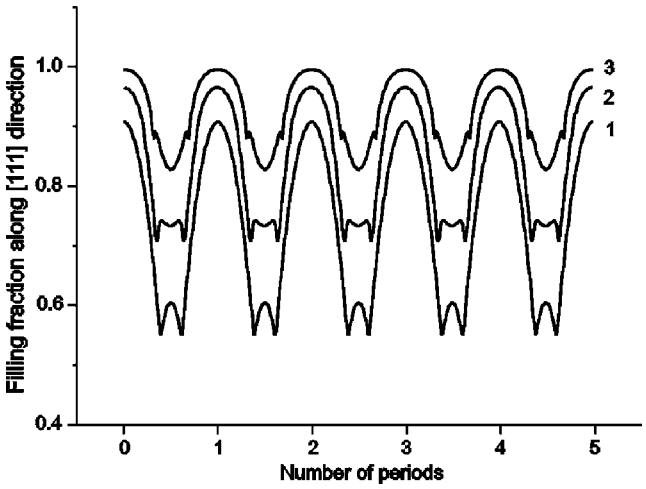

FIG. 8. Spatial profiles of the effective filling function $f_s(z)$ for three values of the sintering coefficient: $\chi=0(1)$, $\chi=0.05(2)$, and $\chi=0.1(3)$.

It should be noted that the observable reflection bands overlap much of the visible spectrum where the dielectric constants ε_m of the GaP and GaN fillers markedly vary with the frequency. For this reason, the calculation of the profiles of the dielectric constants $\varepsilon_s(z)$ from Eq. (5) included the data on the frequency dependencies $\varepsilon_m = \varepsilon_m(\omega)$ of these materials.[24,29] Account was also taken of the possible incomplete filling of the opal pores by calculating their effective dielectric constant ε_{eff} in the Maxwell-Garnett approximation[30]

$$\frac{\varepsilon_{\text{eff}} - \varepsilon_{\text{amb}}}{\varepsilon_{\text{eff}} + 2\varepsilon_{\text{amb}}} = f_m\frac{\varepsilon_m - \varepsilon_{\text{amb}}}{\varepsilon_m + 2\varepsilon_{\text{amb}}}, \tag{7}$$

where ε_m and ε_{amb} are the dielectric constants of the fillers and the ambient, respectively, and f_m is the filling degree, or the volume fraction of the pore fillers. In the case under study, we have $\varepsilon_{\text{amb}}=1$ and f_m relates to the semiconductor filler. The dielectric constant of a-SiO_2 spheres in the opal-semiconductor composites was taken to be $\varepsilon_a=1.98$, found from the spectral analysis of opals filled with water and glycerol. For the inverted structures, this value was $\varepsilon_a=1$, which is the dielectric constant for air.

Unfortunately, actual photonic crystals do not usually possess the structural perfection implied by theoretical models. In particular, the experimental reflectivity at the reflection peak is often less than 50–60%, and the spectral features do not suggest the existence of a 100% reflection plateau that would be characteristic of the photonic stop band of an ideal PhC. In order to include in the model the inevitable and poorly controllable processes of light absorption and scattering associated with the sample imperfection, we added a purely imaginary increment ε'' to the dielectric constant $\varepsilon_s(z)$. The variation in the parameter allowed us to achieve a reasonable agreement between the calculated and experimental spectra in both the shape and the ratio of the background and resonance reflectivities.

TABLE I. The experimental and calculated parameters of the investigated photonic crystals.

	Experimental parameters			Calculated parameters						
Sample	λ_* (nm)	θ_* (deg)	$\Delta E_{FWHM}/E_0$	a_{00} (nm)	χ	η	f_m	ε''	$\Delta E_{gap}/E_0$	q
Bare opal	443	45	0.047	257	0.02	0.93	0	0.048	0.043	0.328
Opal-GaN	530	47	0.063	277	0.05	0.90	0.67	0.092	0.051	–0.241
GaN-inverted opal	413	38	0.117	271	0.05	0.91	0.70	0.090	0.110	–0.528
Opal-GaP			0.174	271	0.03	0.92	0.87	0.240	0.126	–0.558

The numerical computations of the light reflection spectra were made using the transfer matrix method by approximating the filling function by a stepwise function: within each period L, the dielectric medium was considered to be multilayered and made up of N homogeneous dielectric sublayers of the same thickness. The computations provide a steady result practically independent of N at $N>50$. The parameters used in the computations were a_{00}, η, χ, f_m, and ζ_v also (since we studied bulk samples, the back surface and, hence, the parameter ζ_u had no effect on the final results).

C. Multiple Bragg diffraction of light

We have pointed out that the appearance of the doublet structure in the BR spectra at oblique incidence is associated with multiple diffraction in the family of mutually intercepting crystal planes.[23] In our case, the major family of planes is that of the growth (111) planes parallel to the PhC surface. Then the other planes involved in the multiple diffraction must intercept the growth planes at a certain angle. Such inclined planes may be those of the {111} family nonparallel to the sample surface; these will be designated as $(\bar{1}11)$. It is the simultaneous resonance light scattering by the (111) and $(\bar{1}11)$ planes that makes the major contribution to the multiple Bragg diffraction in the lower stop band of the opal-like PhC spectra.[26]

In the "empty lattice" approximation (the dielectric constant modulation is negligible), the dispersion equations for the Bloch modes are

$$\omega = (c/\sqrt{\varepsilon_0})\sqrt{(\mathbf{K}-\mathbf{G}_{hkl})^2} \tag{8}$$

where $\mathbf{K}$ is the Bloch wave vector and $\mathbf{G}_{hkl}(|\mathbf{G}_{hkl}| \equiv G_{hkl})$ are the reciprocal lattice vectors, with the subscripts hkl indicating the families of "atomic" planes (hkl). A coupled solution of Eq. (8) for the light diffraction with the transfer of the wave vector to the vectors $\mathbf{G}_{000}=0$ and $\mathbf{G}_{111}$ of the reciprocal lattice yields the projection $\mathbf{K}$ along the [111] direction along the Z axis

$$K_z = G_{111}/2, \tag{9}$$

which is consistent with the Bragg law of Eq. (1) with the period $d_{111}=a_{00}\eta\sqrt{\frac{2}{3}}$. Note that the formula (9) is also valid over the whole photonic stop band "111," if by K_z we mean the real part of the Z projection of the Bloch wave vector and if we do not restrict ourselves to the empty-lattice approximation.

At certain incidence angles θ, the Bloch mode $\omega=\omega_{\bar{1}11}(K_z)$ formed by the inclined $(\bar{1}11)$ planes is mixed with the attenuating Bloch states $\omega=\omega_{111}(K_z)$ in the 111 photonic band gap due to a periodic modulation of $\varepsilon(\mathbf{r})$ along the $[\bar{1}11]$ direction. As a result, the energy spectrum is renormalized at $K_z \approx G_{111}/2$ in such a way that the condition of Eq. (9) for the ideal 111 band gap is violated producing states in the vicinity of $\omega=\omega_{\bar{1}11}(G_{111}/2)$, associated with the energy transfer in the crystal. Consequently, the reflectivity at this frequency and in its vicinity drops to form a dip in the BR band and a doublet spectrum.[26]

The condition of Eq. (9) is greatly violated at θ values, at which the dispersion curve for the mode $\omega=\omega_{\bar{1}11}(K_z)$ intercepts exactly the 111 photonic stop-band center. The wavelength λ_* for this interception point is[26]

$$\lambda_* = \frac{4a_{00}\sqrt{3}}{4-\eta^{-2}}\sin\theta_*. \tag{10}$$

The experimental values of λ_* and θ_* can be found by approximating the angular displacement of the reflection peaks at oblique incidence ($\theta<45°$), using the Bragg law of Eq. (1) and followed by the extrapolation of theoretical curve (1) over the range $\theta \approx \theta_*$. Then the interception point of the Bragg curve (1) and the experimental curve for the incidence dependence of the doublet minimum must correspond to the values of λ_* and θ_*.[31,32] It is this procedure that we employed in the analysis of the experimental spectra for finding λ_* and θ_*. The obtained values of the two parameters for all the samples are presented in Table I.

The measurement of λ_* and θ_* from multiple Bragg diffraction spectra provides an additional characterization of the PhC structure. The relations (10) that we used essentially represent a structural spectroscopic invariant of a photonic crystal.

IV. DISCUSSION

Figures 3–6 show the theoretical spectra (dashed lines) for small incidence (10°) in s polarization. The calculations were made by varying the values of the major theoretical parameters a_{00}, η, χ, f_m, ε'', and ζ_v. It is important that the fitting provides the only optimal set of values of these parameters, since during the analysis we had to bring to agreement, within the same model, a large number of quantitative and qualitative spectral characteristics.

At the first stage, we fitted the peak positions by varying f_m and the product $a_{00}\eta$, as well as the FWHM of the calculated and measured spectral bands, because these parameters have a determining effect on the reflection band characteristics. Indeed, the position of the Bragg peak is determined by the structure period $L=a_{00}\eta\sqrt{2/3}$ and the average dielectric constant of the photonic crystals. At fixed $\varepsilon_a=1.98$ (see above), the average PhC dielectric constant varies only with the filling factor f_m, which largely determines the reflection band width. With increasing f_m, the modulation percentage of the dielectric constant becomes larger, increasing the stop-band width.

At the second stage, we fitted the details of the reflectance contour by varying the parameters ζ_v and ε'', since they are largely responsible for the relative intensity of the "wings" and asymmetry of the reflection bands. The variation of ζ_v and ε'' modifies the peak positions and band FWHM fitted at the first stage, along with the modification of the general spectral shape. For this reason, the third stage was to minimize the differences between the calculated and experimental spectra by varying the other parameters at constant ζ_v and ε''.

It appeared that the sintering coefficient χ significantly changes the FWHM and position of the Bragg reflection band. At larger χ, the modulation percentage of the PhC dielectric constant decreases (Fig. 8), making the stop band narrower.

The planar approximation used for a quantitative description of the experimental spectra is, in fact, consistent with the one-dimensional (1D) PhC model. In this approach, the spectroscopic data alone cannot provide the values of a_{00} and η individually, but one can find only the spatial period $d_{111}=a_{00}\eta\sqrt{2/3}$, including the product $a_{00}\eta$.

The 3D nature of PhC structures and the deformation of a-SiO_2 spheres were taken into account in the analysis multiple diffraction effects. In this treatment, one can take advantage of the structural invariant of Eq. (10) for a separate determination of a_{00} and η if their product is known and if the parameters λ_* and θ_* have been measured. Thus, the analysis of multiple Bragg diffraction offers an opportunity to characterize the 3D structure of actual photonic crystals.

The observable reflection bands widely vary in shape. In particular, the band asymmetry (the intensity ratio of the long- and short-wavelength wings) for bare opal (Fig. 6) and the opal-GaN composite (Fig. 3) is manifested in opposite ways. In the calculations, the band asymmetry can be controlled by changing the cutoff factor ζ_v.

Normally, the sample surface contains defects because of both the deviation from a regularly planar arrangement of the boundary spheres and the difference in the shapes of individual a-SiO_2 spheres. Moreover, there may be some powder and other contaminants incorporated into the pores during the sample pretreatment. Phenomenologically, this situation could be simulated by introducing a transient surface layer that would vary the relative amplitudes and phases of the Bloch modes inside the PhCs and of the light waves in the ambient. However, the effect of the coefficient also reduces to the change in the amplitudes and phases of the incident and diffracted waves. Therefore, this coefficient can be related not only to the real truncation of the outer a-SiO_2 spheres. More generally, it should be considered as a phenomenological parameter of the boundary conditions, which modifies the BR spectrum.

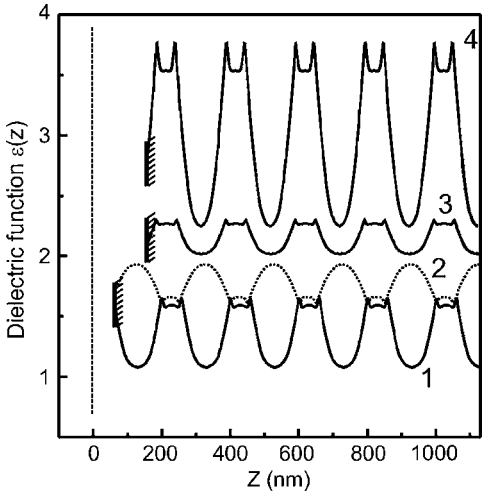

FIG. 9. Profiles of the dielectric constant $\varepsilon(z)$, calculated using the parameters of Table I: opal-GaN composite (curve 1), bare opal (curve 2), GaN-inverted structure (curve 3), opal-GaP composite (curve 4). The z-axis origin lies on the lateral plane tangential to untruncated outer spheroids; the shaded vertical line segments, indicating the outer surface boundary, correspond to the values of the fitting parameter ζ_v.

The values of the fitting parameters best suited for the agreement between the calculated and measured spectra are given is Table I. Figure 9 shows the profiles of the effective dielectric constant for the samples, calculated with these values. For pure opal ($q>0$), the peaks of the dielectric function $\varepsilon(z)$ coincide with the (111) planes crossing the sphere centers. For opal-semiconductor composites ($q<0$), these planes correspond to the $\varepsilon(z)$ dips. The count start along the z coordinate in Fig. 9 lies in the plane having a point contact with the outer untruncated spheres. The shaded vertical line segments, indicating the outer surface boundary, correspond to the values of the fitting parameter ζ_v.

The results on η indicate a noticeable anisotropic shrinkage of the a-SiO_2 spheres, which changes the symmetry of the fcc lattice in opal-like PhCs and can essentially modify their band structure as compared to the available calculations (see, e.g., Ref. 33).

The values of the sintering coefficients χ for the semiconductor-filled opals are larger than those for the initial opals. The opal-GaN composite has the largest χ, which is likely to be associated with the highest (among the samples studied) temperature of the synthesis ($\sim$950 °C), due to which the interpenetration of the spheres is greatest. The f_m values indicate an incomplete pore filling by the semiconductors. Some researchers have reported the possibility to fill up the pores by depositing semiconductor layers onto a -SiO_2 spheres.[34,35] Our computations were based on the assumption of a statistically uniform filling with nanoclusters, and this may be a reason for some discrepancy between the theoretical and experimental spectra.

Table I presents the calculated relative stop-band widths $\Delta E_{gap}/E_0$ of the samples at the incidence of 10°. The values of ΔE_{gap} were calculated as the frequency ranges at 100% reflectivity and $\varepsilon''=0$. The calculated $\Delta E_{gap}/E_0$ and measured $\Delta E_{FWHM}/E_0$ values are in good agreement. Therefore, the PhC stop-band width can be found quite accurately by measuring the BR contour FWHM. Table I also shows the values of the dielectric contrast q at the frequencies of the observable band peaks. It is worth noting the absence of a direct correlation between the results on $|q|$ and $\Delta E_{FWHM}/E_0$. This is because the samples have different sintering coefficients, which essentially change the modulation percentage of the PhC dielectric function.

We have pointed out that the angular dependence of the BR spectra for the opal-GaP composite differs considerably from those for the other composites. This difference is an obstacle to determining, for example, the values of λ_* and θ_*. The measured parameters λ_* and θ_* obey simultaneously relations (1) and (10). Since the largest outer angle cannot exceed 90°, the value of ε_0 consistent with the conditions of the invariant in Eq. (10) appears to be limited[31]

$$\varepsilon_0 \leqslant 1 + \frac{18\eta^2}{(4\eta^2 - 1)^2}$$

At $\eta=1$, the largest value of ε_0 is 3, and the condition for the simultaneous diffraction in the (111) and $(\bar{1}11)$ planes is fulfilled at the grazing angle of the outer incidence. At $\varepsilon_0 > 3$, a simultaneous fulfillment of the Bragg conditions for these planes is possible only with waves excited by sources inside the crystal. For the opal-GaP composites, we have $\varepsilon_0 \approx 3$, and the conditions for multiple diffraction cannot be fulfilled, at least, at the light incidence ($\theta < 70°$) used in our experiments.

V. CONCLUSION

The study of Bragg light reflection spectra of photonic crystals was carried out using opal-GaN and opal-GaP composites as well as GaN-inverted structures with the opal removed from the host crystal. The preliminary characterization of the opal crystals was made from the reflection spectra of pure opals and opals whose pores were filled with immersion liquids (water and glycerol).

The model of an opal-like photonic crystal that we have suggested accounts for the effects of sintering and uniaxial strain of opal a-SiO_2 spheres comprising the crystal, as well as the dispersion of the optical constants of the semiconductor pore fillers in the composites and inverted structures. The model is based on the assumption of a planar space-periodic structure of the material and has been used to analyze the experimental Bragg reflection spectra. As a result, we have found the values of the geometrical and optical parameters of the samples, including those to describe the effects of sintering and strain of the photonic crystal lattice. The detailed analysis of the spectra and their dependencies on the light incidence angles shows that the crystals are compressed along the [111] growth axis and exhibit a considerable sintering of their structural elements. The neglect of these effects in spectral analysis may produce rather large errors in the obtained parameter values of photonic crystals and results in misleading conclusions as to the energy spectrum of the electromagnetic waves.

Of much importance for the characterization of photonic crystals is the concept of structural invariant which establishes an additional relationship between the lattice parameters and the positions of the spectral features. The use of the invariant becomes possible when the reflection spectrum has a doublet structure at certain incidence angles due to multiple Bragg diffraction of light. It is the angular dependence of the spectral position of the dip in the doublet band that carries information necessary for establishing additional restrictions on the parameter values of a photonic structure.

The detailed analysis of the reflection band shapes has been made for small incidence angles when the planar approximation (the 1D photonic crystal approximation) is valid. At rather large angles meeting the multiple diffraction conditions, a full description of the spectra requires the account of the 3D periodicity of the photonic lattice. The approach based on the use of the structural invariant that we have suggested has the advantage of avoiding a detailed quantitative analysis of the reflection contour but relies on the measurement of the incidence angles and the spectral positions of the special point (dip) in the contour. Such measurements can be reliably made in *s*-polarized light, since here the multiple Bragg diffraction effects are much better pronounced than in the *p* polarization. For this reason, we have restricted ourselves to a comparison of the calculated and experimental reflection spectra at small angles ($\theta \approx 10°$), whereas the spectra were measured in *s*-polarized light in a large range of incidence angles. Thus, our study of the Bragg reflection spectra of opal-like photonic crystals has demonstrated capabilities of classical reflection spectroscopy for characterization of such structures and their importance for understanding fundamental mechanisms that describe the interaction of light with spatially periodic media.

ACKNOWLEDGMENTS

The work was supported by the RFBR (Grants No. 05-02-17776 and No. 05-02-17803), the Program of the Presidium of the Russian Academy of Sciences "Low-Dimensional Quantum Structures," and the Contract "PHOREMOST" (FP6/2003/IST-2-511616).

*Also at Daghestan Institute of Physics, 367003 Machachkala, Russia.
†Electronic address: travn@spectr.ioffe.rssi.ru

[1] J. D. Joannopoulos, R. D. Meade, J. N. Winn, *Photonic Crystals: Molding the Flow of Light* (Princeton University Press, Princeton, 1995).
[2] E. Yablonovich, Sci. Am. **285** 47 (2001).
[3] A. Polman and P. Wiltzius, MRS Bull. **26**, 608 (2001).
[4] E. Yablonovitch and T. J. Gmitter, Phys. Rev. Lett. **63**, 1950 (1989).
[5] K. M. Ho, C. T. Chan, and C. M. Soukoulis, Phys. Rev. Lett. **65**, 3152 (1990).
[6] E. Yablonovitch, T. J. Gmitter, and K. M. Leung, Phys. Rev. Lett. **67**, 2295 (1991).
[7] V. N. Astratov, V. N. Bogomolov, A. A. Kaplyanskii, A. V. Prokofiev, L. A. Samoilovich, S. M. Samoilovich, and Yu. A. Vlasov, Nuovo Cimento Soc. Ital. Fis., D **17**, 1349 (1995).
[8] D. J. Norris and Yu. A. Vlasov, Adv. Mater. (Weinheim, Ger.) **13**, 371 (2001).
[9] C. Lopez, Adv. Mater. (Weinheim, Ger.) **15**, 1679 (2003).
[10] A. Reynolds, F. Lopez-Tejeira, D. Cassagne, F. J. Garcia-Vidal, C. Jouanin, and J. Sanchez-Dehesa, Phys. Rev. B **60**, 11422 (1999).
[11] G. Subramania, R. Biswas, K. Constant, M. M. Sigalas, and K. M. Ho, Phys. Rev. B **63**, 235111 (2001).
[12] K. P. Velikov, T. van Dillen, A. Polman, and A. van Blaaderen, Appl. Phys. Lett. **81**, 838 (2002).
[13] T. van Dillen, A. van Blaaderen, and A. Polman, Mater. Today **7**, 40 (2004).
[14] V. N. Bogomolov, V. G. Golubev, N. F. Kartenko, D. A. Kurdyukov, A. B. Pevtsov, A. V. Prokofiev, V. V. Ratnikov, N. A. Feoktistov, and N. V. Sharenkova, Tech. Phys. Lett. **24**, 326 (1998).
[15] V. Yu. Davydov, V. G. Golubev, N. F. Kartenko, D. A. Kurdyukov, A. B. Pevtsov, S. M. Samoilovich, N. V. Sharenkova, P. Brogueira, and R. Schwarz, Nanotechnology **11**, 291 (2000).
[16] V. G. Golubev, V. Yu. Davydov, N. F. Kartenko, D. A. Kurdyukov, V. A. Medvedev, A. B. Pevtsov, A. V. Scherbakov, and E. B. Shadrin, Appl. Phys. Lett. **79**, 1 (2001).
[17] G. Gajiev, V. G. Golubev, D. A. Kurdyukov, A. B. Pevtsov, A. V. Sel'kin, and V. V. Travnikov, Phys. Status Solidi B **231**, R7 (2002).
[18] G. M. Gadzhiev, V. G. Golubev, M. V. Zamoryanskaya, D. A. Kurdyukov, A. V. Medvedev, J. Merz, A. Mintairov, A. B. Pevtsov, A. V. Sel'kin, V. V. Travnikov, and N. V. Sharenkova, Semiconductors **37**, 1400 (2003).
[19] M. S. Thijssen, R. Sprik, J. E. G. J. Wijnhoven, M. Megens, T. Narayanan, A. Lagendijk, and W. L. Vos, Phys. Rev. Lett. **83**, 2730 (1999).
[20] H. Kuchling, *Physik* (VEB Fachbuchverlag, Leipzig, 1980).
[21] V. N. Bogomolov, A. V. Prokof'ev, and A. I. Shelykh, Phys. Solid State **40**, 594 (1998).
[22] Yu. A. Vlasov, V. N. Astratov, A. V. Baryshev, A. A. Kaplyanskii, O. Z. Karimov, and M. F. Limonov, Phys. Rev. E **61**, 5784 (2000).
[23] H. M. van Driel and W. L. Vos, Phys. Rev. B **62**, 9872 (2000).
[24] D. E. Aspnes and A. A. Studna, Phys. Rev. B **27**, 985 (1983).
[25] K. Busch and S. John, Phys. Rev. E **58**, 3896 (1998).
[26] A. V. Sel'kin, in *Nanostructures: Physics and Technology*, Proceedings of the 12th Int. Symp. (St. Petersburg, Russia, 2004), p. 111.
[27] Yu. A. Vlasov, M. A. Kaliteevski, and V. V. Nikolaev, Phys. Rev. B **60**, 1555 (1999).
[28] V. G. Golubev, D. A. Kurdyukov, A. B. Pevtsov, A. V. Sel'kin, E. B. Shadrin, A. V. Il'inskii, and R. Boeyink, Semiconductors **36**, 1043 (2002).
[29] G. Yu, G. Wang, H. Ishikawa, M. Umeno, T. Soga, T. Egawa, J. Watanabe, and T. Jimbo, Appl. Phys. Lett. **70**, 3209 (1997).
[30] J. S. Maxwell Garnett, Philos. Trans. R. Soc. London **203**, 385 (1904).
[31] A. V. Sel'kin, A. Yu. Bilibin, A. Yu. Menshikova, Yu. A. Pashkov, N. N. Shevchenko, and A. G. Bazhenova, Izvestiya RAN **69**, 1111 (2005).
[32] A. V. Sel'kin, in *Nanostructures: Physics and Technology*, Proceedings of the 13th Int. Symp. (St. Petersburg, Russia, 2005), p. 139.
[33] J. F. Galisteo-Lopez, F. N. Garsia-Santamaria, D. Golmayo, B. H. Juarez, C. Lopez, and E. Palacios-Lidon, Photonics Nanostruct. Fundam. Appl. **2**, 117 (2004).
[34] V. G. Golubev, J. L. Hutchison, V. A. Kosobukin, D. A. Kurdyukov, A. V. Medvedev, A. B. Pevtsov, J. Sloan, and L. M. Sorokin, J. Non-Cryst. Solids **299-302** (Part 2), 268 (2002).
[35] F. Garcia-Santamaria, M. Ibisate, I. Rodriguez, F. Meseguer, and C. Lopez, Adv. Mater. (Weinheim, Ger.) **15**, 788 (2003).
[36] The spheres making up the opals consist, in turn, of amorphous SiO_2 nanoparticles with air spaces among them. For this reason, the average dielectric constant of a sphere ε_a differs from that for bulk a-SiO_2.